Available online at www.sciencedirect.com
SCIENCE DIRECT®
Optical Materials 22 (2003) 1–6
OPTICAL Materials
www.elsevier.com/locate/optmat

Controlled size of PbS nanocrystals doped ORMOSIL

N. de la Rosa-Fox [a,*], R. Erce-Montilla [a], M. Piñero [b], L. Esquivias [a]

[a] *Dpto. Física de la Materia Condensada, Facultad de Ciencias, Universidad de Cádiz, Aptdo. 40, Avda, República Saharaui s/n, 11510 Puerto Real (Cádiz), Spain*

[b] *Dpto. Física Aplicada, CASEM, Universidad de Cádiz, Aptdo. 40, 11510 Puerto Real (Cádiz), Spain*

Received 31 May 2002; accepted 11 July 2002

Abstract

PbS semiconductor nanocrystals were grown inside an organically modified silicate (ORMOSIL) matrix prepared by the sol–gel method assisted by high power ultrasounds. Surface capping agent was used to control the growth and aggregation of PbS nanocrystals. The SANS intensity exhibits a crossover at 0.1 nm^{-1}. Data analysis using a two-correlation function indicates a medium-range structure built by PbS nanocrystals (6.5 nm mean crystal diameter) as observed by Transmission electron microscopy. A short-range structure accounts for a fine porosity (1 nm mean pore diameter) of the ORMOSIL matrix in agreement with gas isotherm. Band gap blue-shift confirms the exciton quantum confinement inside the PbS nanocrystals.

1. Introduction

PbS is an attractive semiconductor for the fabrication of quantum dots (QDs) because of its large bulk Bohr exciton radius ($a_B = 18$ nm) [1], as a consequence of its small carrier effective masses ($m^* = 0.1\ m_e$) and large optical dielectric constant ($\varepsilon = 17$). The strong quantum confinement regime is thus easily obtained, and the ground-state absorption edge can be tuned over a wide wavelength range (from the near infrared to the visible) [2,3], since the gap in QDs of R radius scales [4] as $1/R^2$. Moreover, due to the smaller surface/volume ratio, surface states should play a minor role in PbS quantum dots when it is compared to the II–VI semiconductor nanocrystals. These surface trap states are responsible of a decline in the non-linear optical behaviour of the material (e.g., photodarkening) [5]. Recently, PbS QDs doped glasses have been used as saturable absorbers for solid-state lasers [6].

The performance of these materials is influenced by the small size of crystals. Thus, the crystal sizes and their size distribution are critical parameters to improve the quantum confinement effects [7]. In this work we present, the synthesis of PbS/SiO_2 composites based on the sol–gel method assisted by high power ultrasounds (sonogel) [8]. This method consists basically in the promotion of the chemical reactions to form the hybrid organic–inorganic silica network as matrix. The use of these sonogels as matrices takes the advantage of

* Corresponding author. Tel.: +34-956-016322/6317; fax: +34-956-016288.
E-mail address: nicolas.rosafox@uca.es (N. de la Rosa-Fox).

0925-3467/02/$ - see front matter
PII: S0925-3467(02)00101-5

their specific textural characteristics (denser and microporous) [9], as well as their good optical properties, thermal, mechanical and chemical stability [10]. Afterwards the PbS crystal growth is provoked by solution supersaturation. To control this precipitation process we have used a surface capping agent (SCA), specifically 3-mercaptopropyl group that form strong covalent bonds with Pb sites [11]. In such a situation, the SCA molecules passivate the Pb surface sites on the sub-critical PbS crystal and prevent their oxidation. An excess of uncoordinated S sites act as potential surface traps which produce important steric effects on the closer silica network [9]. The final size of the PbS particle is then controlled by adjusting the relative concentrations of SCA and sulphide [12,13].

2. Experimental methods

2.1. Synthesis and preparation

We used silanol-terminated PDMS with quoted average molecular weight of 400–700, and TMOS, for preparing hybrid organic–inorganic host matrices. The chemical reactions were shortened by using high power ultrasounds (20 kHz, 600 W) to form "sono-ormosils" [14]. As a matter of fact, the ultrasounds energy dose influences the polymerization rate, polydispersity and chain breakage, obtaining shorter gelation times, higher density matrices, smaller pore radii and narrower pore-size distribution [8,15].

In order to ensure the homogeneous incorporation of PDMS chains into the silica inorganic network, a two-step hydrolysis was used and described as follows:

(1) TMOS was first partially hydrolysed with HNO_3 catalyst in a molar ratio of TMOS:H_2O:HNO_3 of 1:0.84:0.026. The organic polymer PDMS was added in a molar ratio TMOS:DMS of 1:0.19, where the organic fraction in the hybrid material has been expressed as a function of the dimethyl-siloxane monomer, DMS. At this step, the resulting solution (sol A) received 320 J cm^{-3} ultrasounds energy, and was translucide due to submicro or even nanophase separation, as a result of thermodynamic incompatibility between the organic and inorganic precursors. It was kept in hermetically closed containers at 50 °C for 24 h and, along this time, it evolved into transparent solution suspecting that covalent bonds have been formed between silanol groups of PDMS chains and the inorganic constituent.

(2) Hydrolysis of sol A was completed subsequently by adding nitric acid water, with a molar ratio TMOS:H_2O:HNO_3 of 1:3.36:0.0015, with 500 J cm^{-3} of ultrasound energy, and the transparent homogeneous sol here obtained was suitable for doping.

From this point, we proceeded to mix lead acetate (PbAc) and thioacetamide, inside the organic–inorganic silica sol, to get 0.5, 1, 2, and 4 wt.% PbS nanocrystals doped ormosils. Here, aggregation and subsequent precipitation of lead sulphide was help it by using 3-mercaptopropyl tetramethyl silane which acts as a SCA of the small PbS colloidal particles formed in the early stages of the process, thus promoting a highly dispersed dot population inside the matrix. To avoid its decomposition in acidic medium the solution pH was increased. Different PbS and SCA content were used, and they are called as XRY, where X is the PbS wt.% contents and Y is the molar ratio between SCA and PbS added to the solution.

The gelation time ranged from 1 to 60 min. The doped sono-ormosils were aged at room temperature during 5 days closed air tight, to strengthen, and subsequently dried slowly for another 15 days by putting several holes on the cover. By this way, yellow coloured gels were obtained which turn progressively into orange, red, brown and dark colour transparent gels. However, someone of them stopped its colour transition at yellow or red, depending both on the PbS composition and the crystallite size.

2.2. Thermal treatment

The thermal behaviour of the dried samples was studied by thermogravimetric analysis as previously reported [9]. The main weight losses are produced in the temperature ranges of 60–110 °C and 175–220 °C, the former step is due to the solvents evaporation and the second one to the organic polymer decomposition and PbS oxidation.

These results permitted us to schedule the thermal treatment of the samples. consisting in heating the sample under inert atmosphere, from room temperature to 100 °C for 3 h. The visual aspect of the samples alters from yellow to dark red for composites and remains transparent for the undoped matrix, this change in the colour shade reveals the subsequent growth of the PbS crystal.

2.3. Textural and structural characterization

The textural characteristics of the resultant gels were studied by means of N_2 physisorption isotherms at 77K in an automatic device Sorptomatic-1990 of FISONS. Powdered samples were previously degassed at 100 °C for 3 h.

Transmission electron microscopy (TEM) was performed as direct observation technique by using a JEM 2000EX from JEOL of the Science and Technology Central facilities in the University of Cadiz. Size distribution were calculated by direct method on the micrograph over 70 crystal spots.

SANS experiments on V4 work station at HMI (Berlin), were performed by using 6.02 Å as neutron wavelength and using 1, 4 and 16 m as sample-detector distance, in order to cover a q range of 0.036–3.6 nm^{-1}. Standard programs were used for the data reduction, e.g. normalisation of the efficiency of the two-dimensional detector, masking of the detector cells near the beam stop, and subtraction of the scattering by the empty cell and of the electronic background [16]. The isotropic scattering was calculated by the radial average in all directions in such a way to improve the intensity yield. The macroscopic coherent scattering cross-section in units of inverse centimetres was calculated by using the scattering data from the water (1 mm thick cell).

3. Results and discussion

Fig. 1 shows the results from nitrogen physisorption measurements for the undoped matrix and the outlined composites. In all cases, a type I isotherm features the microporosity without hysteresis loop due to the absence of capillary condensation on the mesopore wall. As can be seen the adsorption is produced practically below 0.2 relative pressure, this behaviour reveals the fine porosity of the undoped matrix, giving 0.5 nm mean pore radius calculated from the adsorption branch. This result takes the advantage of the ultrasonic treatment in the liquid mixture (sonogel) [8,9,17]. Similar features for the composite samples indicate the conservation of such microporous structure (Table 1). However, the observed increase of the adsorbed volume for 0.5R32 sample accounts for the steric effects of the SCA molecules. Whereas, for the other ones the decrease of the adsorbed volume run parallel with the PbS content.

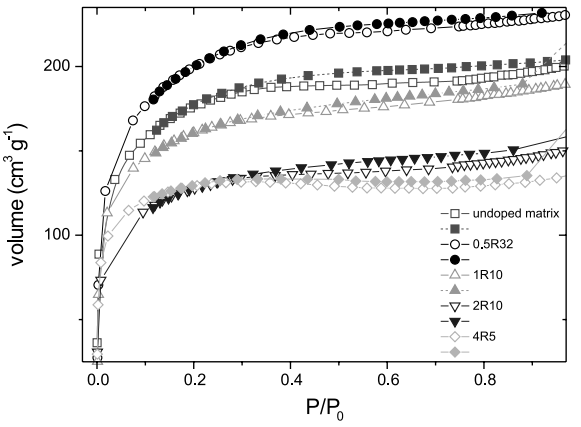

Fig. 1. N_2 physisorption isotherms as a function of both PbS and SCA content. Open symbols correspond to the adsorption branch and the solid symbols to the desorption one.

TEM micrograph in Fig. 2 shows that the PbS nanocrystals in the 0.5R32 sample are homogeneously distributed into the matrix. The mean crystal size is 6.5 ± 0.6 nm as calculated from its size distribution in the inset of Fig. 2. This range of crystal size suggests that PbS crystals are formed prior to gelling, and the bridge formed by the SCA on the particle surface controls its further growth. Moreover, the ormosil matrix surrounding the PbS crystals prevents their subsequent growth and oxidation.

The corrected SANS intensity curves are shown in Fig. 3. In all cases, it is possible to discern two regions from the well-defined crossover point around $q = 0.1$ nm^{-1}. For high q-values a wide

Table 1
Textural parameters calculated from N_2 physisorption isotherms at 77 K

Sample	Specific surface area S ($m^2\,g^{-1}$)	Porous volume V_p ($cm^3\,g^{-1}$)	Pore size $4V_p/S$ (nm)	Apparent density ρ_a ($g\,cm^{-3}$) ± 0.05	Density from physisorption ρ'_a ($g\,cm^{-3}$)
Undoped matrix	616	0.3237	2.10	1.29	1.28
0.5R32	677	0.4830	2.86	1.03	1.07
1R10	542	0.4676	3.46	1.08	1.09
4R5	414	0.2101	2.02	1.55	1.51

Sample code is *XRY*, *X* being the PbS wt.% and *Y* the SCA/PbS molar ratio. Apparent density ρ_a was calculated from geometrical dimensions of the parallelepiped pieces with a slide calliper (1/20 mm accuracy). $1/\rho'_a = V_p + 1/\rho_s$ ($\rho_s(SiO_2) = 2.2\ g\,cm^{-3}$).

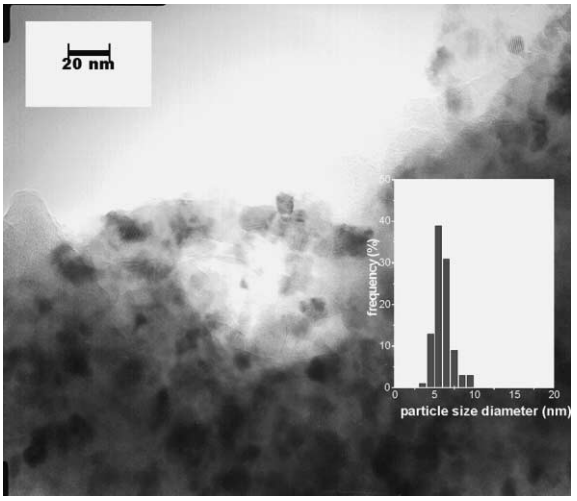

Fig. 2. TEM micrograph of 0.5R32 sample showing an homogeneous distribution of PbS particles with mean crystal size of 6.5 ± 0.6 nm. Inset shows the size distribution calculated over 70 spots on the micrograph.

plateau is apparent, which is characteristic of fine well-shaped scatters homogeneously distributed as a fine porosity could produce. On the other hand, the increase of the signal at low q-values is characteristic of larger polydisperse particles, as could be produced by the polymer cross-links or/and the PbS nanocrystals. The scattering from the undoped matrix is also included, inset in Fig. 3. In the absence of crystals, a smooth broad peak develops at $q = 0.5\ nm^{-1}$, which accounts for the short-range order of the pores.

It is well known that crystals in gels grow by a diffusion-controlled process. In such a situation, the concentration gradient around the crystal depletes a surrounding volume larger than the crystal and where is not possible to find another crystal [21]. According to this idea, the experimental intensities were fitted by the two-correlation model proposed by Debye and Bueche [18] and Debye et al. [19] where the scattering cross-section behaves as

$$\frac{d\Sigma}{d\Omega}(q) = \frac{A_1}{(1+q^2a_1^2)^2} + A_2 \exp\left(-\frac{q^2a_2^2}{4}\right) \qquad (1)$$

where the correlation lengths a_1 and a_2 represent the medium-range and short-range fluctuations, respectively, in the scattering length density. The parameters A_1 and A_2 are related with the corresponding volume fraction of each phase. Eq. (1) can be considered the form factor $P(q)$ of the heterogeneties, then the total scattering cross-section become $I(q) = \Phi \cdot P(q) \cdot S(q)$, Φ and $S(q)$ being the particle number density and structure factor, respectively. The structure factor $S(q)$ was evaluated assuming the Percus–Yevick hard-sphere model, and using the expression of Ashcroft and Lekner [20]. This approach of the SANS patterns involves the existence of a depleted region around the PbS crystals, where the growth of another crystal is inhibited [21].

The structure factor accounts for the interparticle interference terms which could be produced either by crystals or pores. The results of such a fitting are shown in Table 2 and the fitted curves from $I(q)$ are drawn in Fig. 3. The undoped matrix does not fit (inset Fig. 3) such twofold correlated structure, as can be deduced from the noisy signal at low-q. Then, the observed increase of intensity

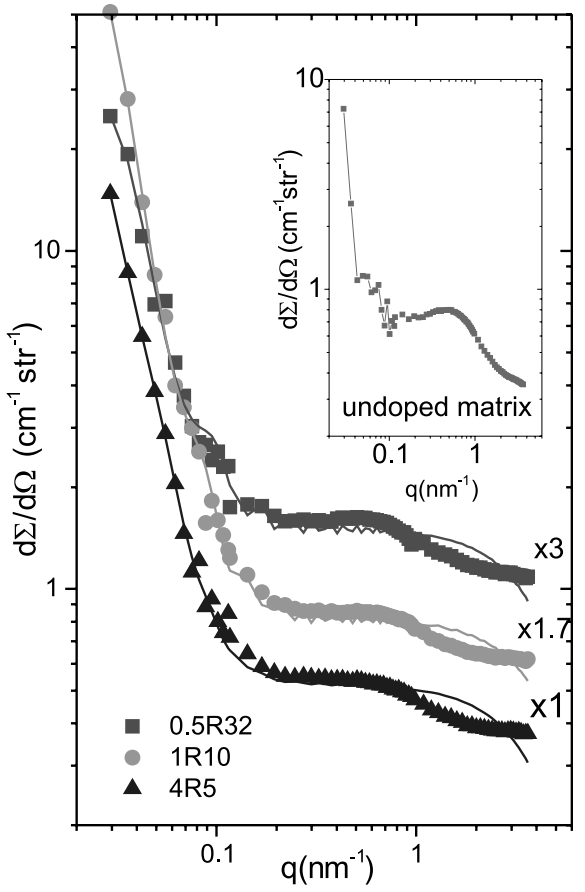

Fig. 3. SANS scattered intensities from 0.5R32, 1R10 and 4R5 samples. The solid lines correspond to the non-linear least-square fit from $I(q)$. Inset shows the undoped matrix sample. Sample–detector distance was set at 1, 4 and 16 m with a $\lambda = 0.6$ nm as neutron wavelength. Scattering vector modulus is $q = (4\pi \sin\theta/2)/\lambda$, θ being the scattering angle. Some contribution of the incoherent scattering coming from the ormosil matrix can be noticed at the end of the curves ($q > 2$ nm^{-1}), this fact mask probably the Porod behaviour in this q-region ($I \propto q^{-4}$).

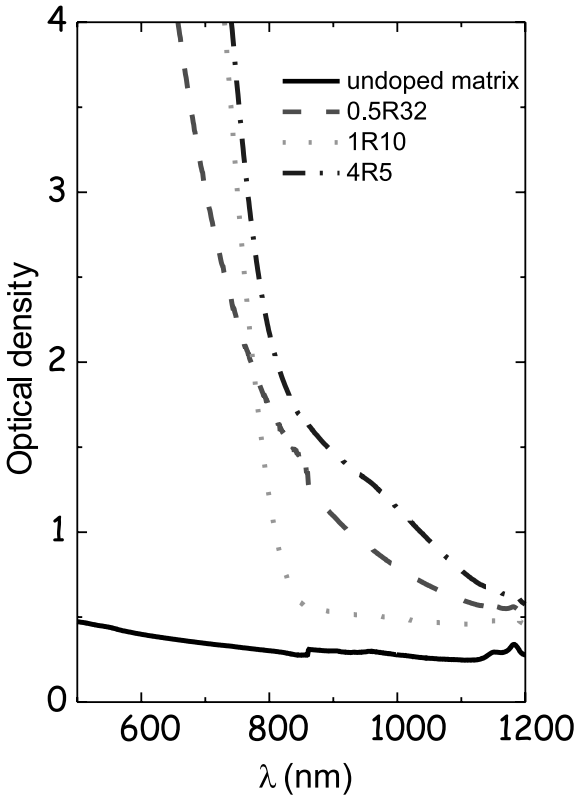

Fig. 4. Optical absorption spectra obtained by transmission at room temperature from the outlined samples 1 mm thick. The undoped matrix has been plotted as transparent reference.

must be due to the local heterogeneties produced by the polymer cross-linking [22] with the silica network at the boundary of the SCA molecules surrounding the PbS nanocrystals.

From Table 2, it can be stated, that the crossover point at $q = 0.1$ nm^{-1} resolves the twofold structure for the doped samples. Thus, A_1 and a_1 grow with the PbS content. These values are shockingly high against those of A_2 and a_2, in spite of the bigger scattering length density of the matrix/pores (short-range) relative to that of the PbS/matrix one

Table 2
Structural parameters from the fitted experimental intensities by using the two-correlation function to the Debye–Bueche model according to Eq. (1)

PbS-ormosil	A_1 (cm^{-1})	a_1 (nm)	TEM (nm)	Depleted region (nm)	A_2 (cm^{-1})	a_2 (nm)
0.5R32	9.8	22.5	6.5 ± 0.5	8	0.52	0.50
1R10	81.1	35.6	10.5 ± 0.5	12	0.49	0.38
4R5	104.2	44.0	13.5 ± 0.5	15	0.56	0.85

(medium-range). Moreover, the comparison between the high a_1 values against the TEM results (inset Fig. 2 and Table 2), confirm the existence of a depleted region surrounding the crystal that control the dot density. These results account for a dot density higher than those for QDs in Schott filters [21] due to the smaller depleted region. We attribute the underestimation of a_2 values as regard to the pore size calculated from physisorption (see Table 1), to the incoherent scattering contribution for $q > 1\ \mathrm{nm}^{-1}$, in the absence of which the knee of the fit curves at $q = 2\ \mathrm{nm}^{-1}$ will shift to smaller values, thus accounting for big pores.

UV–vis spectra are shown in Fig. 4. They present, the characteristic blue-shift from the bulk PbS band gap at 0.41 eV as the main signature of the exciton quantum confinement. The absence of sub-banding structure could be due to temperature quenching or to the fact that some forbidden optical transitions are allowed when $R/a_B \cong 0.5$. On the other hand, the long tail of the 0.5R32 sample accounts for the large hole traps due to the high SCA content that produces an excess of uncoordinated sulphide sites.

4. Conclusions

In conclusion, the size of the PbS QDs can be controlled and stabilised via sol–gel by using a SCA and assisted by high power ultrasounds. These results are suitable to obtain strong confinement effects in these PbS QDs embedded in sono-ormosil matrix. Also high dot density with small depleted region surrounding the PbS nanocrystals can be obtained.

These results are promising to obtain strong quantum confinement ($R < a_B$) of the PbS quantum dots and, as a consequence, large non-linear optical behaviour can be expected. In this way UV–vis spectra show the characteristic blue-shift from the bulk PbS band gap (0.41 eV, 3200 nm) as the main signature of the exciton confinement.

Finally, it is possible to conclude the good agreement between the different characterisation techniques, taking the advantage of the SANS measurements, with a well-defined crossover point between both microstructures.

Acknowledgements

This work has been supported in Spain by the project MAT98-0798 of the CICyT and for the SANS measurements in the HMI of Germany by the TMR/LSF access program ERBFMGE CT950060 of the European Commission. Spanish authors belong to the TEP-0115 group of the Junta de Andalucía.

References

[1] N.F. Borrelli, J.C. Luong, Proc. SPIE 866 (1987) 104.
[2] Y. Wang, N. Herron, J. Phys. Chem. 91 (2) (1987) 257.
[3] Y. Wang, N. Herron, J. Phys. Chem. 92 (1988) 4988.
[4] L. Efros, A. Efros, Sov. Phys. Semicond. 16 (1982) 772.
[5] U. Woggon, in: Optical Properties of Semiconductors Quantum Dots, Springer Tracts Modern Physics, vol. 136, Springer, Berlin, 1997.
[6] K. Wundke, S. Pötting, J. Auxier, A. Schülzgen, N. Peyghambarian, N.F. Borrelli, Appl. Phys. Lett. 76 (2000) 10.
[7] N.F. Borrelli, D.W. Hall, H.J. Holland, D.W. Smith, J. Appl. Phys. 61 (1987) 5399.
[8] E. Blanco, L. Esquivias, R. Litrán, M. Piñero, M. Ramírez-del-Solar, N. de la Rosa-Fox, Appl. Organomet. Chem. 13 (1999) 399.
[9] R. Erce-Montilla, M. Piñero, N. De la Rosa-Fox, A. Santos, L. Esquivias, J. Mater. Res. 16 (9) (2001) 2572.
[10] J.D. Mackenzie, J. Sol–Gel Sci. Tech. 2 (1994) 81.
[11] M. Guglielmi, A. Martucci, E. Menegazzo, G.C. Righini, S. Pelli, J. Ficky, G. Vitrant, J. Sol–Gel Sci. Tech. 8 (1997) 1017.
[12] A. Martucci, J. Fick, J. Scell, G. Battaglin, M. Guglielmi, J. Appl. Phys. 86 (1) (1999) 79.
[13] F. del Monte, Y. Xu, J.D. Mackenzie, J. Sol–Gel Sci. Tech. 17 (2000) 37.
[14] K. Morita, Y. Hu, J.D. Mackenzie, J. Sol–Gel Sci. Tech. 3 (1994) 109.
[15] N. de la Rosa-Fox, L. Esquivias, J. Zarzycki, Difus. Def. Data 53&54 (1987) 363.
[16] E. Hoinkis, Langmuir 12 (1996) 4299.
[17] A. Craievich, N. de la Rosa-Fox, E. Blanco, M. Piñero, M. Ramírez-del-Solar, L. Esquivias, NanoStruct. Mater. 5 (1995) 363.
[18] P. Debye, M. Bueche, J. Appl. Phys. 20 (1949) 518.
[19] P. Debye, H.R. Anderson Jr., H. Brumberger, J. Appl. Phys. 28 (1957) 179.
[20] N. Ashcroft, J. Lekner, Phys. Rev. 145 (1966) 83.
[21] G. Banfi, V. Degiorgio, B. Sepeit, J. Appl. Phys. 74 (1993) 6925.
[22] E. Geissler, F. Horkay, A.M. Hecht, C. Rochas, Polymer 38 (1) (1997) 15.